Nanofiber Network Ion-Exchange Membranes

Jonghyun Choi,[†] Kyung Min Lee,[†] Ryszard Wycisk,[†] Peter N. Pintauro,*[,†] and Patrick T. Mather*[,‡]

Department of Chemical Engineering, Case Western Reserve University, Cleveland, Ohio 44106, and Syracuse Biomaterials Institute, Biomedical and Chemical Engineering Department, Syracuse University, Syracuse, New York 13244

Received March 11, 2008
Revised Manuscript Received May 7, 2008

Introduction. DuPont's Nafion perfluorosulfonic acid membrane has been extensively studied for use in hydrogen/oxygen and direct methanol proton-exchange membrane (PEM) fuel cells,[1] but it readily dehydrates at elevated temperatures and low humidity, it is a poor methanol barrier, and its mechanical properties are suspect. Historically, research on Nafion replacements has proceeded along two lines: the use of new polymers with covalently attached acidic fixed-charge groups, e.g., sulfonated poly(imides), polyphosphazenes, and poly(arylene ethers)[2] and the creation of heterogeneous polymer blends and polymer/inorganic composites (e.g., Nafion−Teflon blends and sulfonated poly(ether ketone)/zirconium phosphonate composites).[3,4] To ensure high proton conductivity, high ion-exchange capacity polymers were utilized, but these polymers swelled excessively in water (with a loss in mechanical properties) and were brittle when dry. Although the use of polymer/particle composites did improve membrane water retention (where water is needed for fixed charge group dissociation and the creation of hydrophilic protogenic pathways), there was no substantial improvement in proton conductivity at low humidity conditions.[4]

More recently, researchers have focused on manipulating the polymer morphology at the nanometer scale, as an additional means of improving membrane function and mechanical properties. The most common approach has been to utilize ion-containing block copolymers, based, for example, on sulfonated polystyrene or sulfonated poly(arylene ether sulfone).[5,6] Unfortunately, for many ion-containing block copolymers, there is no guarantee of high-level microscale (long-range) organization of the phase-separated nanodomains, and therefore the potential advantages of using these materials to improve proton conductivity in a PEM fuel cell have not been fully realized. Additionally, solution-casting of block copolymers into membranes is problematic due to the complicated effect of solvent/polymer interactions on the final morphology and the requirement of polymer solubility in the solvent.

We report here on a completely new approach to ion-exchange membrane preparation, where a three-dimensional interconnected network of electrospun polyelectrolyte nanofibers is created and then the interfiber voids are filled with an inert/uncharged polymer. Such a phase-separated nanomorphology is not unlike the desired/ideal structure in a block copolymer system, but there is more flexibility in the fabrication approach. Thus, the polyelectrolyte, fiber diameter, fiber volume fraction, and inert polymer can be chosen/fixed independently. The uncharged (hydrophobic) polymer which surrounds each nanofiber restricts fiber swelling in water and provides mechanical strength to the membrane, thus permitting the fibers to have a fixed-charge concentration much greater than that which is practical in a homogeneous ion-exchange membrane. Also, the interconnecting nanofiber structure ensures optimum utilization of percolation pathways of the ionomer (i.e., there will be no isolated domains of charged polymer or dead-end nanochannels). Although the focus of the present paper is on a proton conducting membranes for fuel cell applications, the nanofiber network membranes described below can be used for other purposes, such as electrodialysis separations, sensors, and industrial electrolyses.

Electrospinning has been used to create a variety of new materials, including high strength composites,[7] filtration media,[8] medical and pharmacological products,[9] and textiles.[10] Fabrication of electrospun nanofibers of polyelectrolyte solutions was initially considered impossible due to strong repulsive interference forces between ionogenic groups,[11] but several of these materials have been electrospun recently, such as poly(2-acrylamido-2-methyl-1-propanesulfonic acid),[12] poly(acrylic acid),[13] chitosan,[14] and sulfonated poly(ether ether ketone ketone).[15] There are only a handful of reports in the literature on electrospinning of fibrous proton-conducting mats. Nah et al.[16] reported that ionic liquid embedded mats from Nafion (for use as electromechanical transducers) showed a proton conductivity 3 times greater than that of dense Nafion films. Laforgue et al.[17] prepared mats from electrospun Nafion/poly(vinyl alcohol) blends and compared their proton conductivity to that of homogeneous Nafion films while Chen et al.[18] described electrospinning of Nafion and Nafion−poly(acrylic acid) solutions (electrospinning neat Nafion was unsuccessful).

In the present study, a nanofiber composite network ion-exchange membrane was fabricated using a four-step procedure: (i) electrospinning a nanofiber mat of ion-exchange polymer, (ii) compacting the mat to increase the volume density of fibers in the final membrane, (iii) forming polymer welds between intersecting fibers to create a three-dimensional interconnecting network, and (iv) filling the void space between fibers with an inert polymer. The resulting membrane nanostructure is shown schematically in Figure 1.

Results and Discussion. A mat of ionomeric nanofibers was electrospun from a solution of 25 wt % sulfonated poly(arylene ether sulfone),[2] hereafter denoted as sPAES (Figure 1), in dimethylacetamide. High molecular weight sPAES polymer with an ion-exchange capacity (IEC) of 2.5 mmol/g and an intrinsic viscosity of 0.72 dL/g was prepared by polycondensation of three monomers, according to the procedures outlined in the Supporting Information. Large mats (16 cm × 6 cm) of electrospun fibers with a uniform mat thickness and fiber density were prepared using a rotating drum collector that oscillated laterally (horizontally). Mats were compacted/densified under pressure to increase the volume density of nanofibers, with no change in fiber diameter. To create interconnecting protonic pathways, intersecting fibers were welded by exposing the densified sPAES mat to dimethylformamide (DMF) vapor at 25 °C for 18 min.

Optical photographs and SEM images of the surface of a sPAES nanofiber mat at three stages of membrane fabrication are shown in Figure 2. For the initial (as-spun) mat, the volume fraction of fibers was 0.11−0.18, the mat thickness was 114 μm, and the number-average fiber diameter was 110 nm. (The

* Corresponding authors: Tel 216-368-4150, Fax 216-368-3016; e-mail pnp3@case.edu (P.N.P); Tel 315-443-8760, e-mail ptmather@syr.edu (P.T.M.).
[†] Case Western Reserve University.
[‡] Syracuse University.

10.1021/ma800551w CCC: $40.75
Published on Web 06/10/2008

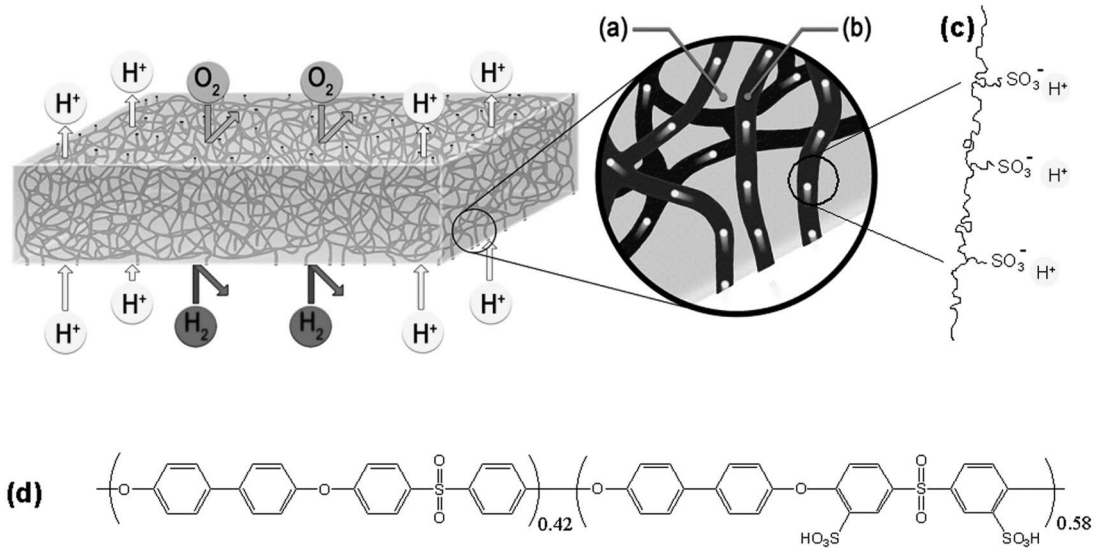

Figure 1. Schematic diagram of the nanofiber network composite fuel cell proton-exchange membrane. The inset shows the polymer matrix (a) which restricts swelling of the nanofibers and imparts mechanical strength to the membrane. The water-swollen fiber network (b) is composed of a sulfonated cation-exchange polymer shown (c) schematically and (d) in actual chemical structure form.

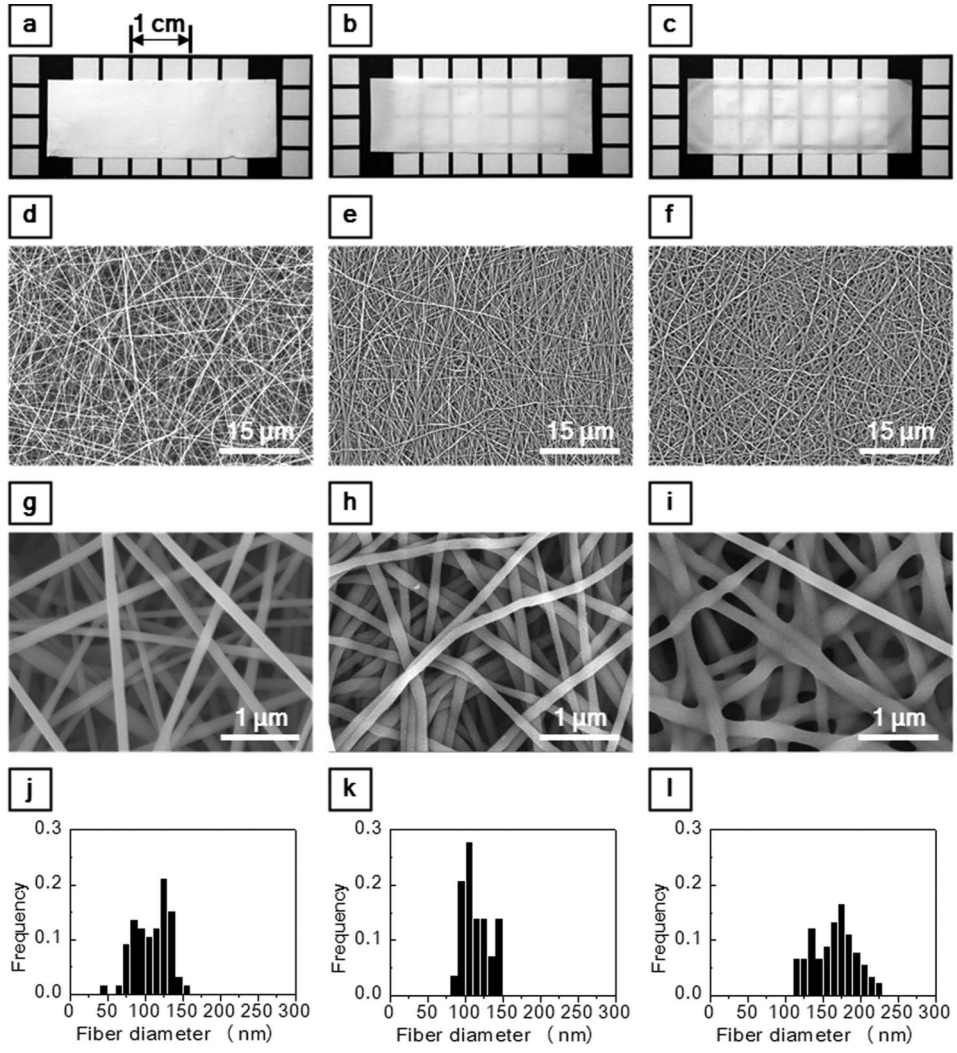

Figure 2. Electrospun fiber mat of sulfonated poly(arylene ether sulfone) at three stages of transforming the mat into an ion-exchange membrane: initial (as-spun) mat (a, d, g, j), mat after fiber densification (b, e, h, k), and mat after densification and fiber welding (c, f, i, l). (a−c) are optical photographs, (d−f) are scanning electron micrographs of the mat surface at a magnification of 2000×, (g−i) are scanning electron micrographs of the mat surface at a magnification of 30 000×, and (j−l) are histograms of the fiber diameter distribution, as determined from the 30 000× SEMs.

fiber diameter distribution ranged from 40 to 160 nm, as shown by the histogram in Figure 2j.) The fiber density was calculated as the weight of the dry mat relative to that of a dry homogeneous sPAES film of the same size and thickness. The

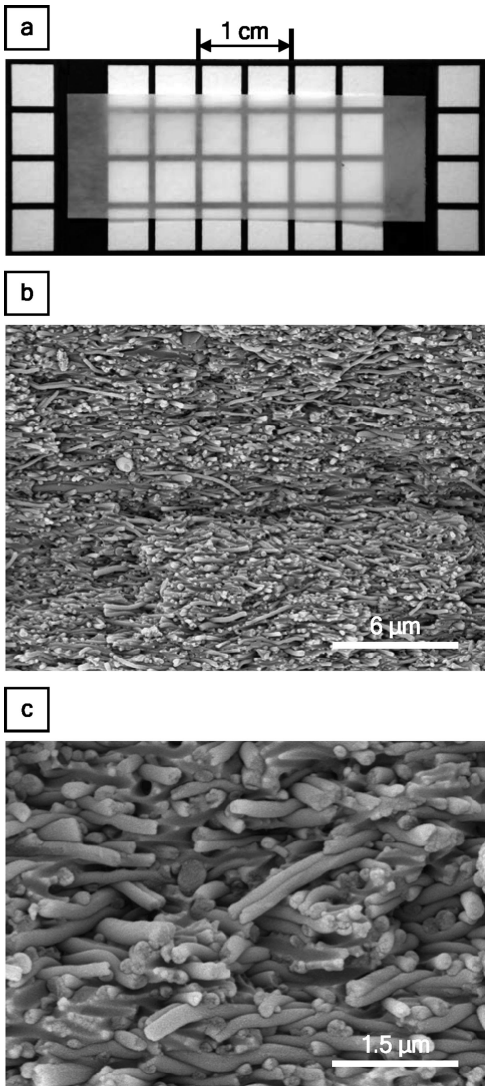

Figure 3. Nanofiber composite membrane formed by compacting, welding, and impregnating an electrospun mat of sulfonated poly(arylene ether sulfone) with Norland Optical Adhesive (NOA) 63. (a) Actual photograph of the NOA63-impregnated (and UV-cured) mat. (b, c) Scanning electron micrographs of membrane cross section of the NOA63 composite membrane at magnification of 5000× (b) and 30 000× (c). The membrane thickness was 39 μm.

densified mat in Figure 2 was created by mechanically compaction at 13 000 psi for 3 min at 25 °C, where the fiber volume fraction increased to 0.64, the mat thickness decreased to 32 μm, and the average fiber diameter was essentially unchanged at 114 nm. After compaction and fiber welding, the volume fraction of fibers and the average fiber diameter increased to 0.73 and 165 nm, respectively, with essentially no change in mat thickness (35 μm). Details of fiber electrospinning, mat compaction, and fiber welding are given in the Supporting Information.

After welding, the sPAES nanofiber mat was impregnated with Norland Optical Adhesive (NOA) 63, a solvent-less photocurable urethane-based prepolymer, and exposed to UV light, as described in the Supporting Information. A top-view optical photograph and freeze-fractured SEM cross-section images of the final nanofiber composite membrane are shown in Figure 3. Nanofibers are clearly seen, with uniformly dense NOA 63 polymer filling completely the interfiber voids. The nanofiber network membrane had a more desirable morphology and better mechanical properties than a UV-cured polymer

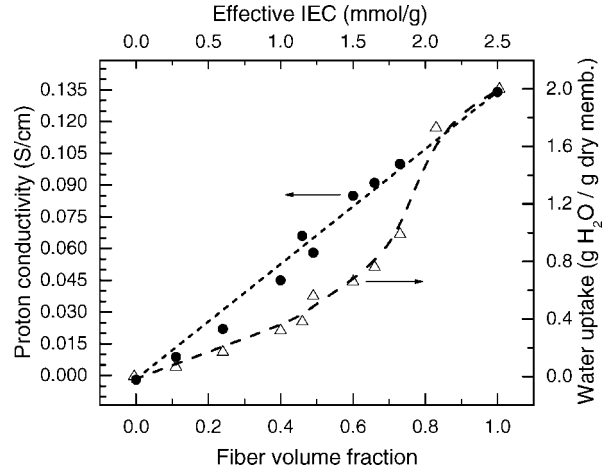

Figure 4. Proton conductivity and water uptake at 25 °C of nanofiber composite membranes as a function of fiber volume fraction prior to embedding. The fibers were composed of 2.5 mmol/g sulfonated poly(arylene ether sulfone) and the inert matrix was UV-cured NOA63.

blend; for example, a membrane composed of 70 wt % sPAES and 30 wt % NOA63 that was cast from dimethylacetamide solvent was brittle when dry and highly phase separated with isolated 5−10 μm domains of NOA63, as revealed by SEM analysis.

A series of preliminary characterization experiments were performed on impregnated mats of different fiber volume fractions (11−80%) and the results were contrasted with similar measurements on neat films of sPAES (cast from dimethylacetamide) and UV-cured NOA63. In-plane proton conductivity and equilibrium water uptake (swelling) at 25 °C for nanofiber composite membranes of different fiber volume fraction (as measured before NOA63 impregnation) are presented in Figure 4. The data are also plotted against the effective membrane ion-exchange capacity, which is equal to the product of the fiber volume fraction and fiber polymer ion-exchange capacity. A fiber volume fraction of 1.0 denotes a homogeneous film of 2.5 mmol/g sulfonated poly(arylene ether sulfone), and a volume fraction of 0.0 corresponds to an uncharged NOA63 film. Proton conductivity increased linearly with fiber volume fraction in the composite membranes and showed no percolation threshold, contrary to what is generally observed for immiscible conductor/insulator polymer blends. From a limited number of through-plane conductivity experiments, it was concluded that the fiber network morphology and the proton conductivity were isotropic; i.e., at 55% and 70% fiber volume fractions, the in-plane and through-plane conductivities were identical (within experimental error) at 0.064 and 0.086 S/cm, respectively.

The importance of the compaction step during membrane fabrication, to increase fiber volume fraction and thereby increase membrane conductivity, is obvious from Figure 4 (i.e., the conductivity at 40% fiber volume fraction is about half that at 80%). The need for interfiber welding after compaction was confirmed by comparing the in-plane proton conductivity of embedded mats (of equal fiber volume fraction) with and without welding, where the conductivity was about 10% higher for the welded membranes (e.g., 0.058 S/cm with welding vs 0.053 S/cm without welding for an embedded film with a fiber volume fraction of 48%).

In contrast to the conductivity data, a nonadditive behavior with respect to composition was seen in the water-uptake results. At fiber volume fractions below 0.80, membrane swelling was less than expected on the basis of the amount of sulfonated polymer in the membrane. This deviation from the additivity

rule was expected due to the ability of the NOA63, which surrounds all sulfonated polymer nanofibers, to restrict fiber swelling. When the fiber volume fraction was greater than ≈0.80, water uptake was directly proportional to the volume fraction of sulfonated polymer, indicating either weak interconnectivity of the NOA63 matrix or its insufficient strength to restrict swelling of the nanofibers. The dependence of water uptake on effective membrane ion-exchange capacity (the shape of the water uptake curve in Figure 4) is similar to that for a series of homogeneous sPAES films of different IEC (see data in Table 1 of ref 19).

The measured properties of the nanofiber network membranes compare very well to those of a commercial Nafion 117 sample, whose proton conductivity and water swelling at 25 °C were 0.09 S/cm (both in-plane and through-plane) and 0.35 g H_2O/g, respectively. Additionally, the embedded nanofiber membranes exhibited good mechanical properties; the ultimate tensile strength for a nanofiber network membrane with a fiber volume fraction of 50% was 28 MPa as compared to 15 MPa for Nafion 117 (both membranes were equilibrated in air at 25 °C and 35% relative humidity).

Steady-state oxygen permeability experiments (at 25 °C and 50% relative humidity) were performed to check for membrane defects and to assess the gas barrier property of the nanofiber composite membranes (an important and required attribute for fuel cell applications). The oxygen permeability in a membrane with a nanofiber volume fraction of 0.60 and a thickness of 45 μm was 0.18 barrers. This permeability was unexpectedly low, given the nanofiber volume fraction, an O_2 permeability of 0.53 barrers for a homogeneous 2.5 mmol/g sulfonated poly(arylene ether sulfone) film (cast from dimethylacetamide with a dry thickness of 45 μm), and a permeability of 0.038 barrers for a dense NOA63 film that was UV-cured for 2 h at 25 °C. Additionally, the oxygen barrier property of the nanofiber composite membrane was more than 50 times higher than that of a commercial Nafion 117 sample (9.4 barrers, as measured after membrane pretreatment by boiling for 1 h each in 3% H_2O_2 and 1.0 M H_2SO_4).

Acknowledgment. The authors gratefully acknowledge Eric Fossum of Wright State University (who assisted in the polymer synthesis) and the financial support of the U.S. Department of Energy, Energy Efficiency and Renewable Energy Program (Grant DE-FG36-06GO16030).

Supporting Information Available: Details of the fabrication and characterization of the nanofiber composite network ion-exchange membranes. This material is available free of charge via the Internet at http://pubs.acs.org.

References and Notes

(1) Gasteiger, H. A.; Mathias, M. F. In *Proton Conducting Membrane Fuel Cells III, Electrochemical Society Proceedings*; Murthy, M., Fuller, T. F., Van Zee, J. W., Gottesfeld, S., Eds.; ECS: Pennington, NJ, 2005; Vol. *2002-31*, p 1.
(2) Hickner, M. A.; Ghassemi, H.; Kim, Y. S.; Einsla, B. R.; McGrath, J. E. *Chem. Rev.* **2004**, *104*, 4587–4611.
(3) Lin, J.; Lee, J. K.; Kellner, M.; Wycisk, R.; Pintauro, P. N. *J. Electrochem. Soc.* **2006**, *153*, A1325–A1331.
(4) Alberti, G.; Casciola, M. *Annu. Rev. Mater. Res.* **2003**, *33*, 129–154.
(5) Serpico, J. M.; Ehrenberg, S. G.; Fontanella, J. J.; Jiao, X.; Perahia, D.; McGrady, K. A.; Sanders, E. H.; Kellogg, G. E.; Wnek, G. E. *Macromolecules* **2002**, *35*, 5916–5921.
(6) Wang, H.; Badami, A. S.; Roy, A.; McGrath, J. E. *J. Polym. Sci., Part A* **2007**, *45*, 284–294.
(7) Chronakis, I. S. *J. Mater. Proc. Technol.* **2005**, *167*, 283–293.
(8) Gopal, R.; Kaur, S.; Ma, Z.; Chan, C.; Ramakrishna, S.; Matsuura, T. *J. Membr. Sci.* **2006**, *281*, 581–586.
(9) Zhang, Y.; Lim, C. T.; Ramakrishna, S.; Huang, Z. M. *J. Mater. Sci.: Mater. Med.* **2005**, *16*, 933–946.
(10) Lee, S.; Obendorf, S. K. *Text. Res. J.* **2007**, *77*, 696–702.
(11) Park, W.; Jeong, L.; Yoo, D.; Hudson, S. *Polymer* **2004**, *45*, 7151–7157.
(12) Kim, S. J.; Lim, J. Y.; Kim, I. Y.; Lee, S. H.; Lee, T. S.; Kim, S. I. *Smart Mater. Struct.* **2005**, *14*, N16–N20.
(13) Li, L.; Hsieh, Y. L. *Polymer* **2005**, *46*, 5133–5139.
(14) De Vrieze, S.; Westbroek, P.; Van Camp, T.; Van Langenhove, L. *J. Mater. Sci.* **2007**, *42*, 8029–8034.
(15) Li, X.; Hao, X.; Xu, D.; Zhang, G.; Zhong, S.; Na, H.; Wang, D. *J. Membr. Sci.*, in press.
(16) Nah, C.; Kwak, S. K.; Kim, N.; Lyu, M. Y.; Hwang, B. S.; Akle, B.; Leo, D. J. *Key Eng. Mater.* **2007**, *334*−*335*, 1001–1004.
(17) Laforgue, A.; Robitaille, L.; Mokrini, A.; Ajji, A. *Macromol. Mater. Eng.* **2007**, *292*, 1229–1236.
(18) Chen, H.; Snyder, J. D.; Elabd, Y. A. *Macromolecules* **2008**, *41*, 128–135.
(19) Kim, Y. S.; Dong, L.; Hickner, M. A.; Glass, T. E.; Webb, V.; McGrath, J. E. *Macromolecules* **2003**, *36*, 6281–6285.
(20) Lin, J.; Wycisk, R.; Pintauro, P. N.; Kellner, M. *Electrochem. Solid-State Lett.* **2007**, *10*, B19–B22.

MA800551W